

Structural Behaviour of the Corbelled Vaults of Ta Prohm

Sreeja Chandran, A. Meher Prasad and Devdas Menon

Indian Institute of Technology, Department of Civil Engineering, Chennai, India

ABSTRACT: The present study deals with the structural collapse observed in the first three enclosure walls of the Ta Prohm temple, which is one of the major temples at Angkor Wat, the largest temple complex in the world. This complex is at present in a state of ruin and structural collapse. The first three enclosure walls at Ta Prohm are vaulted gallery dry stone block masonry structures, in which the main vaulted roof is made by corbelling large stone blocks to make an arch form, resulting in a continuous vault. The different failure modes observed in these structures and the lack of understanding the exact reason behind these structural distresses has led to the present study.

1 INTRODUCTION

Ta Prohm is one of the major temples at Angkor Wat, the largest temple complex in the world. The temple was constructed in the 12th century as a Buddhist monastic complex. The present study addresses the structural collapse of the first three enclosure walls of the temple, which are vaulted gallery masonry structures. The possible causes underlying the observed structural collapse are investigated adopting finite element formulations.

2 STRUCTURAL CONSTRUCTION

The layout of the main temple comprises four rectangular wall enclosures, contained within a large site of 700m × 1000m. These enclosure walls are vaulted gallery masonry structures, in which the main vaulted roof is made by corbelling large stone blocks to make an arch form, resulting in a continuous vault. In general, the material used is sandstone, but in the second enclosure, laterite stone has been extensively used in many areas. The second and third enclosures are bigger than the first enclosure, and they comprise vaulted galleries combined with side aisles. The main vaulted roof is supported on a continuous wall on one side and a row of pillars with lintel beams on the other side. These pillars also support side aisles along with another row of pillars. In the second enclosure, the wall is on the outside and the two rows of pillars on the inside, while in the third enclosure, the wall is on the inside with the two rows of pillars on the outside. Fig.1 shows the sectional elevation of the first and second enclosure walls at Ta Prohm. These vaulted structures, made entirely of dry stone masonry, apparently remained in good stable condition for a few hundred years.

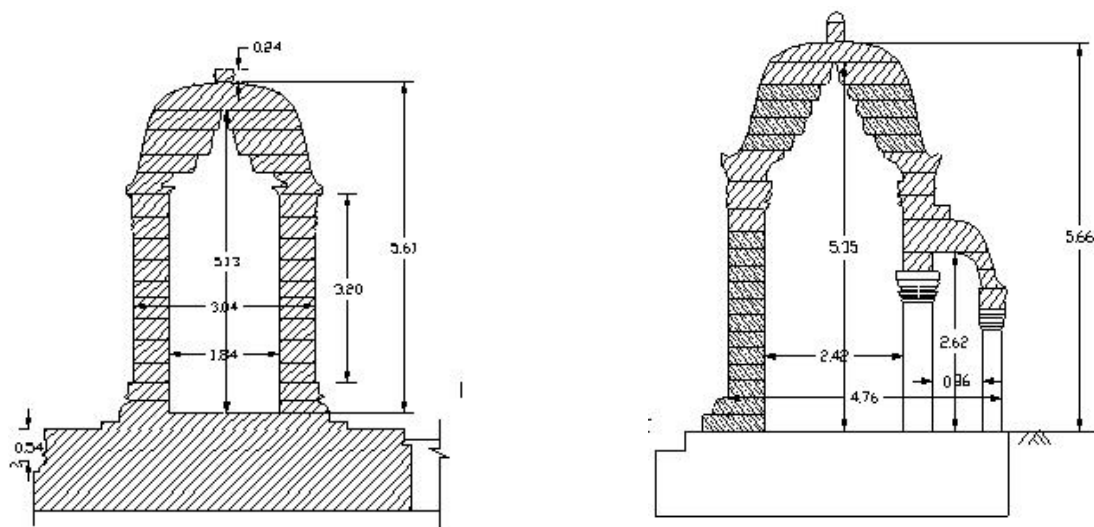


Figure 1 : Sectional elevation of the first two enclosure walls at Ta Prohm temple complex

3 STRUCTURAL FAILURE AT THE SITE

The typical structural failures observed in enclosure walls at the site are depicted pictorially in Fig. 2. Failures are mostly attributed to dislodging of stones at the vaulted roof. In the case of enclosure walls with side aisles, the lateral movement of the pillars have rendered the stability of the structure extremely vulnerable, and caused the entire roof to cave in.



Figure 2 : Typical structural failures observed in the enclosure walls

4 STRUCTURAL BEHAVIOUR

It is established that although the vaulted structures are stable under normal gravity loads and nominal wind loads, they are prone to instability when the foundations are disturbed. Failure possibilities due to footing settlement have been ruled out by geotechnical experts (Menon et al, 2004). It was noted that the main Angkor Wat temple with a higher loading intensity showed satisfactory behaviour in poorer soil stratum than that at Ta Prohm. All evidence suggests that the foundation disturbances have been caused by the growth of extensive vegetation (including trees like *Dipterocarpus Alatus* and *Tetrameles Nudiflora* with large adventitious roots).

5 FINITE ELEMENT MODELLING

In order to study the structural behaviour under footing movements the first and second /third enclosure walls are modelled in two dimensions using the commercial finite element package ANSYS 5.6. The stone blocks and the interface are modelled following the true geometry of the

structure. The stone blocks are modelled using PLANE 42 elements available in the ANSYS element library. These are two-dimensional quadratic four noded elements with two translational degrees of freedom at each node. Plane stress behaviour is assumed. The interface is modelled using the non-linear contact elements in order to capture the possible sliding and large rotational movements at the joints. The Contact 172 and Target 169 contact pair elements are used for modelling the interface. The resistance to horizontal sliding is attributed only to the frictional resistance of the interface. A contact model generally involves the specification of the contact surfaces, defining the motion of the contact surface (rigid/flexible), defining the type of contact element stiffness matrix (symmetric/un-symmetric), defining the contact algorithms and defining the nature of the contact. In the present study, the contact occurs between stone blocks of equal stiffness, which can be considered as two deformable surfaces in contact. As far as the contact stiffness matrices are concerned the symmetric stiffness matrix is computationally inexpensive. But this method is not applicable for contact problems where friction has to be taken into account. But the capability of the numerical package to use a symmetrisation algorithm in order to help in solving most of the frictional contact problems using solvers for symmetric matrices, a symmetric stiffness matrix assumption is adopted. From a set of available contact algorithms, the Augmented Lagrangian algorithm is used for finding the contact status. This algorithm usually leads to better conditioning and is less sensitive to the magnitude of contact stiffness. A realistic standard frictional surface assumption is made where the normal stress equals zero if separation occurs. The Contact 172 and Target 169 contact pair elements in the ANSYS library, which are capable to incorporate all the explained properties, are used for modelling the interface. The first enclosure wall is discretized into a relatively regular mesh of 1084 quadratic elements and 557 contact elements. Similarly in the second enclosure wall a total number of 997 quadratic elements and 354 contact elements are being used for discretization. A coefficient of friction of 0.5 is assumed for the interface (Giordano et al, 2002). Stone blocks are considered as linear elastic and isotropic. The material properties of sandstone are obtained based on tests done on a number of samples from the contemporary temple at the Preah Khan temple. The material parameters are listed in Table 1.

Table 1: Material Properties of Sandstone

| Young's Modulus (MPa) | Poisson's Ratio | Density kg/m ³ | Compressive strength (MPa) | Flexural Strength (MPa) |
|-----------------------|-----------------|---------------------------|----------------------------|-------------------------|
| 20000 | 0.2 | 2300 | 19-21 | 5.5 |

The failure of corbelled arches occurs mainly due to sliding of the stones when the limiting frictional force between two adjoining stones is exceeded. This depends on (i) the magnitude of the applied force tangential to the joint and, (ii) the magnitude of frictional force that can be developed, which is a product of the coefficient of friction and magnitude of normal force. Here, the sliding force between two stones is equal to the horizontal thrust. Moreover, the magnitude of the normal thrust and hence frictional force reduces progressively with respect to the stones that are higher up in the corbelled arch. In the present study, the stability of the structure under gravity loading is analysed. Subsequently the behaviour of the structure due to various types of footing movements (as the possible cause of collapse of the structure is attributed to footing movement due to root penetration) is studied by a non-linear step-by-step analysis. For convenience, two typical symmetrical foundation movements are studied:

- (a) Outward rotation at the base and
- (b) Inward rotation at the base.

The possible failure modes are captured by gradually increasing the inward/outward rotations at the base of the structure. The results obtained are discussed below.

6 RESULTS AND DISCUSSIONS

6.1 Gravity Load Analysis

The static analysis of both enclosure walls under normal gravity load shows satisfactory performance. A maximum normal stress of 0.7 MPa is observed in the case of the first enclosure walls and of 0.4 MPa in the case of second enclosure walls. Both values are well below the compressive strength (about 20 MPa) of the stone units used. It is noted in the analysis that the maximum shear stress (of the order 0.03 MPa) is well below the frictional resistance (coefficient of friction X Normal thrust) of the interface. It is thus evident that the dry block masonry construction has very high factor of safety under normal loading conditions. Fig. 3a and b represents the vector plots of the principle stress component of the first and second enclosure walls respectively under dead weight. It is clear from the plots that the location maximum stress coincides with the base of the arches and with the base of the supporting walls in the case of first enclosure walls. Whereas in the case of second enclosure walls the higher stress levels are observed at the base of the supporting wall and at the top of the inner pillar of the side aisle.

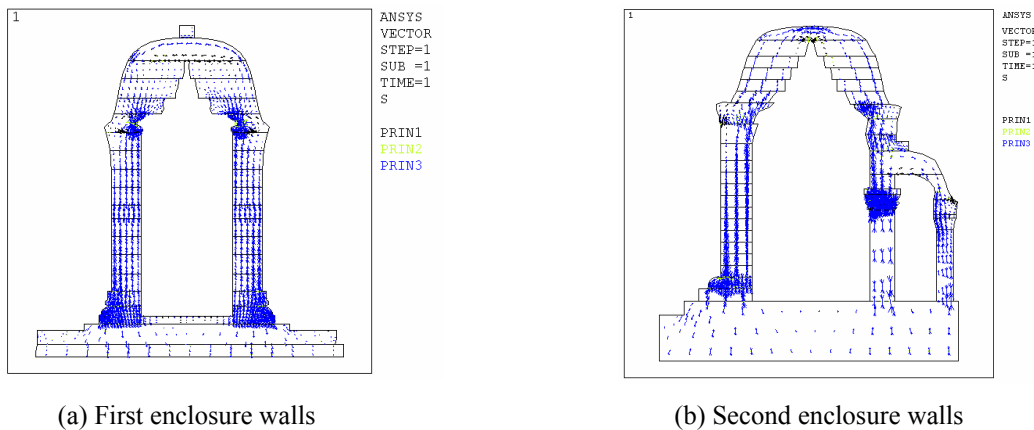


Figure 3 : Principal stress plots under gravity loading

6.2 Effect of outward rotation

The footing movements are represented as symmetric outward rotations. The outward rotations in general, gradually reduce the resistant sections until they behave like hinges. The subsequent subsections explain the behaviour of the first two enclosure walls under outward rotations at the base.

6.2.1 First enclosure walls

The results related to the effect of outward rotation in the first enclosure walls are shown in Fig.4. Part (a) of the figure illustrates the deformed shape contours corresponding to an outward rotation of 7.06×10^{-3} radians at the base of the structure. The analysis proves that the structure is extremely vulnerable to outward rotation at the base. Even rotations of the order of 10^{-4} radians are found to be enough to open up the horizontal joints and lead to large rotational movements of the masonry blocks.

The reason behind this sort of failure can be inferred from the part (b) of the figure. The figure shows a plot between applied rotations at the base and normal thrust. It should be noted that a gradual increase in the outward rotation reduces the normal thrust on the structure, which in turn reduces the frictional resistance of the unit interfaces. At the considered section 'X' the vertical stress value showed a drop down from 4000 Pa to zero on an increase in the outward rotation from 0.5×10^{-4} radians to 3.5×10^{-4} radians. This reduction in the normal stress leads to large rotations of the blocks and possible collapse of the structure by toppling of the stones (Fig. 4a).

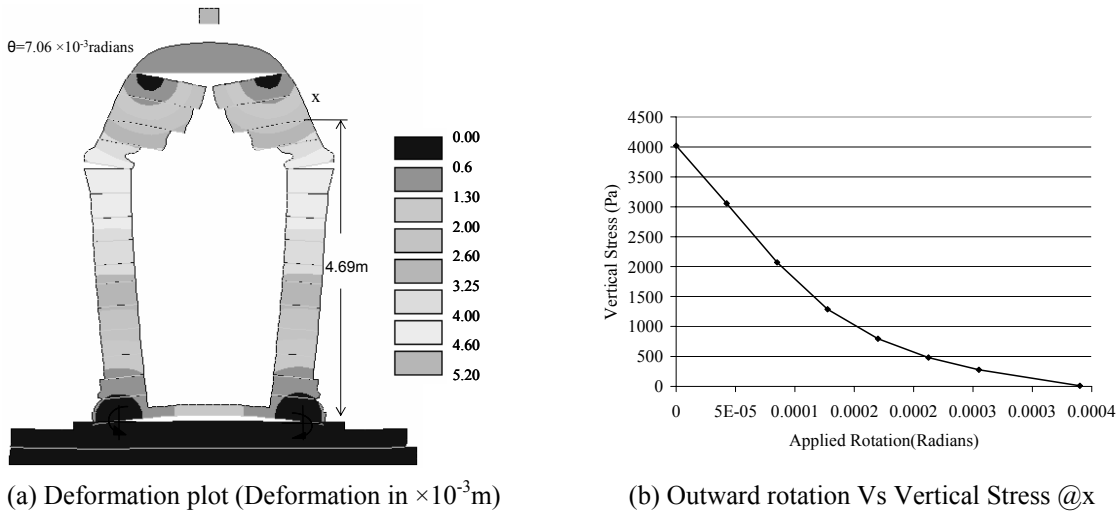


Figure 4 : Effect of outward rotation on first enclosure

6.2.2 Second/ third enclosure walls

The second and third enclosure walls will be showing same structural behaviour under symmetric loading conditions. The behaviour of the second/third enclosure walls under outward rotation is shown in Fig. 5. From Fig. 5a it is clear that the failure of the structure is attributed to the lateral movement of the supporting pillars and the subsequent sliding of the vaulted roof from the support. This is the most common failure mode observed at Ta Prohm. This has been pictorially captured and represented in Fig. 2. As explained earlier, part (b) of the figure makes it clear that the reduction in the normal stress due to a gradual increase in the outward rotation is the main reason behind the observed collapse. The normal stress reduced from 0.8MPa to 0.05MPa as the outward rotation is increased from 0.5×10^{-3} radians to 3.5×10^{-3} radians.

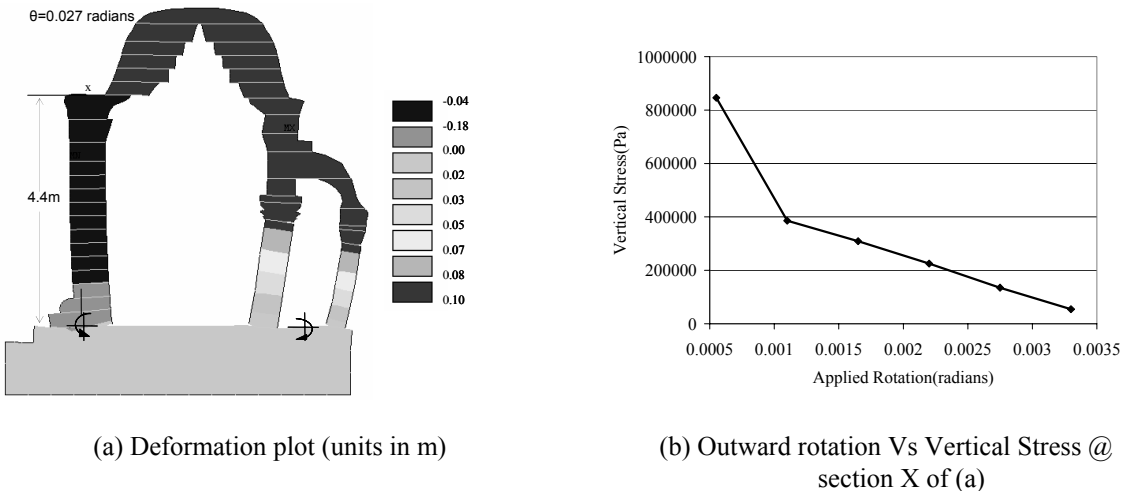


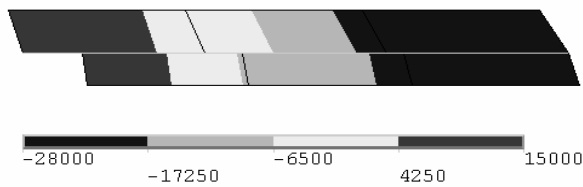
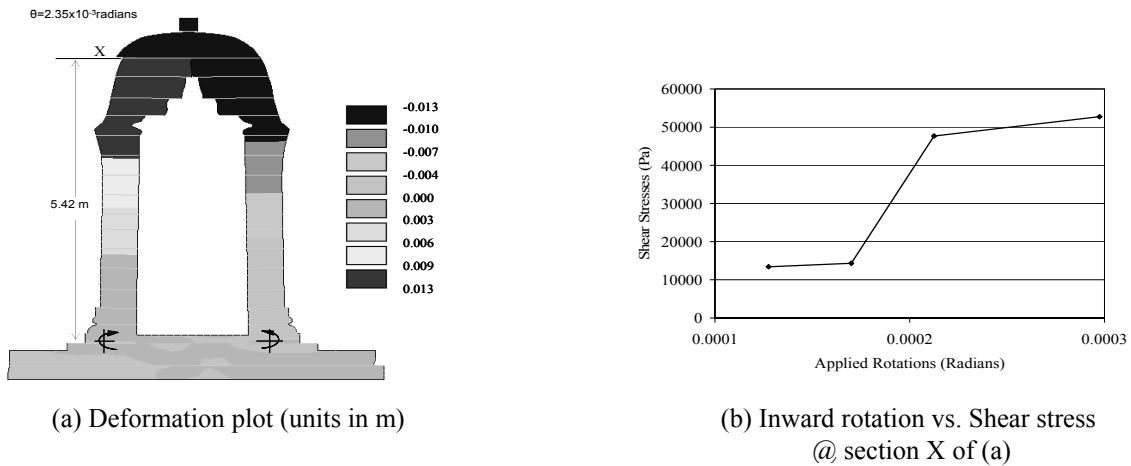
Figure 5 : Effect of outward rotation on second/third enclosure

6.3 Effect of inward rotation

The footing movements are represented as symmetric inward rotations. Inward rotations in general, cause an increased shear stress in the structure. The subsequent subsections address the structural behaviour of the first three enclosure walls at Ta Prohm under inward rotations.

6.3.1 First enclosure walls

The results related to the effect of inward rotation in the first enclosure walls are shown in Fig. 6. In the case of inward rotation, the failure is controlled by the shear/sliding resistance of the interface. As expected, it is seen that a gradual increase in the inward rotation results in an increase in the shear stress in the structure (Figs. 6b). This increased shear on the dry masonry leads to the inward sliding of the vaulted roof units (Fig. 6a), where the normal thrust is the least. Figure 4.17 part (c) explains the normal stress distribution at the failed section X under normal gravity loading. It is clear from the plots (c) that the maximum normal stress at the section is 0.028MPa which will ensure maximum shear strength of 0.014 MPa under the considered coefficient of friction of 0.5. Under normal gravity loading the shear stresses at the section falls below this value. But as we increase the base rotation the shear stress at the section is also increases and it crosses the shear strength of the section leading sliding failure of the section. It is evident from part (B) of Fig. 6 that as we increases the base rotation from 0.0001 radians to 0.0002 radians there is a rapid increase in the shear stress from 0.01MPa to 0.05 MPa which will obviously lead to the sliding failure of the section.



(c) Normal stress distribution @ section X of (a) under gravity loading
 Figure 6 : Effect of Inward rotation on b First enclosure (units in

6.3.2 Second /third enclosure walls

Fig. 7 explains the behaviour of second/third enclosure walls under inward rotation. The behaviour of the structure is exactly similar to that of first enclosure walls. Part (a) of the figure shows the observed failure pattern where as part (b) shows a plot between the applied rotation and the shear stress at the failed section X. As explained already the failure is attributed to the inward sliding under increased shear stresses. Part c of the figure shows the normal stress distribution at the section under normal gravity loading. From the plots it is clear that as we increase the base rotation from 0.001 radians to further there is a considerable increase in the shear stress which exceeds the shear strength of the section ($0.5 \times$ Normal stress).

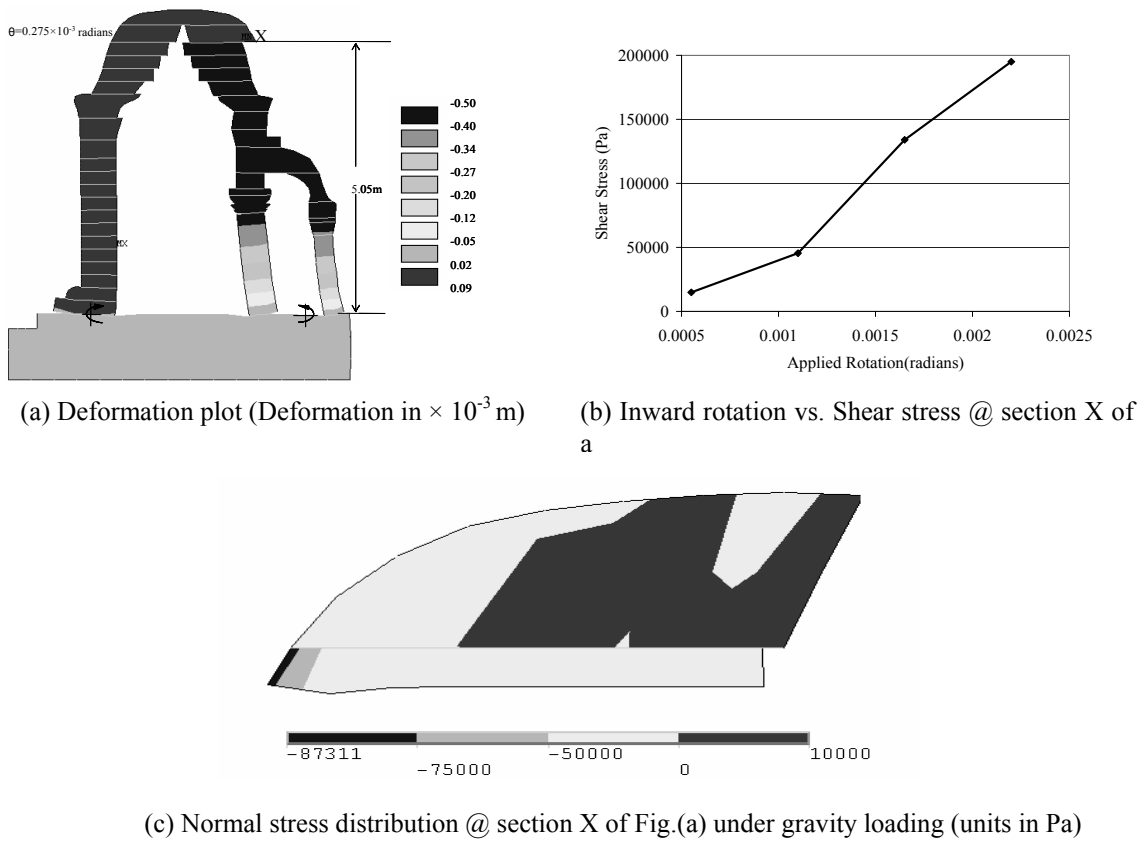


Figure 7 : Effect of Inward rotation on the second/third enclosure

6.4 Effect of variation in the coefficient of friction

The coefficient of friction at the unit interface is varied from 0.3 to 0.7 in the case of a standard contact. The significant changes in the failure modes are plotted in Figs. 8 and 9. A rough contact assumption is made where the sliding failure mode is restricted through an infinite coefficient of friction. The assumption of infinite coefficient of friction is not valid under practical circumstances. This case is studied only to get an insight to the failure modes once the sliding motion of the blocks is prevented. It is noted that under an assumption of infinite frictional resistance and foundation movements the structural failure is due to the opening up of horizontal joints. Under limited frictional resistance the sliding resistance of the interface governs most of the failure modes of the structure. As the frictional resistance is increased to 0.7 sliding modes of failure is giving way to rotational failure and opening up of horizontal joints.

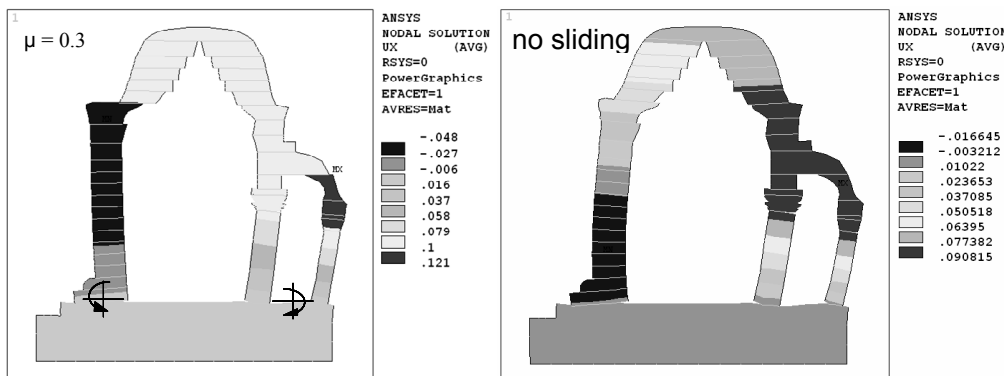


Figure 8 : Different failure modes in the second/third enclosure walls under outward rotation with different coefficient of friction

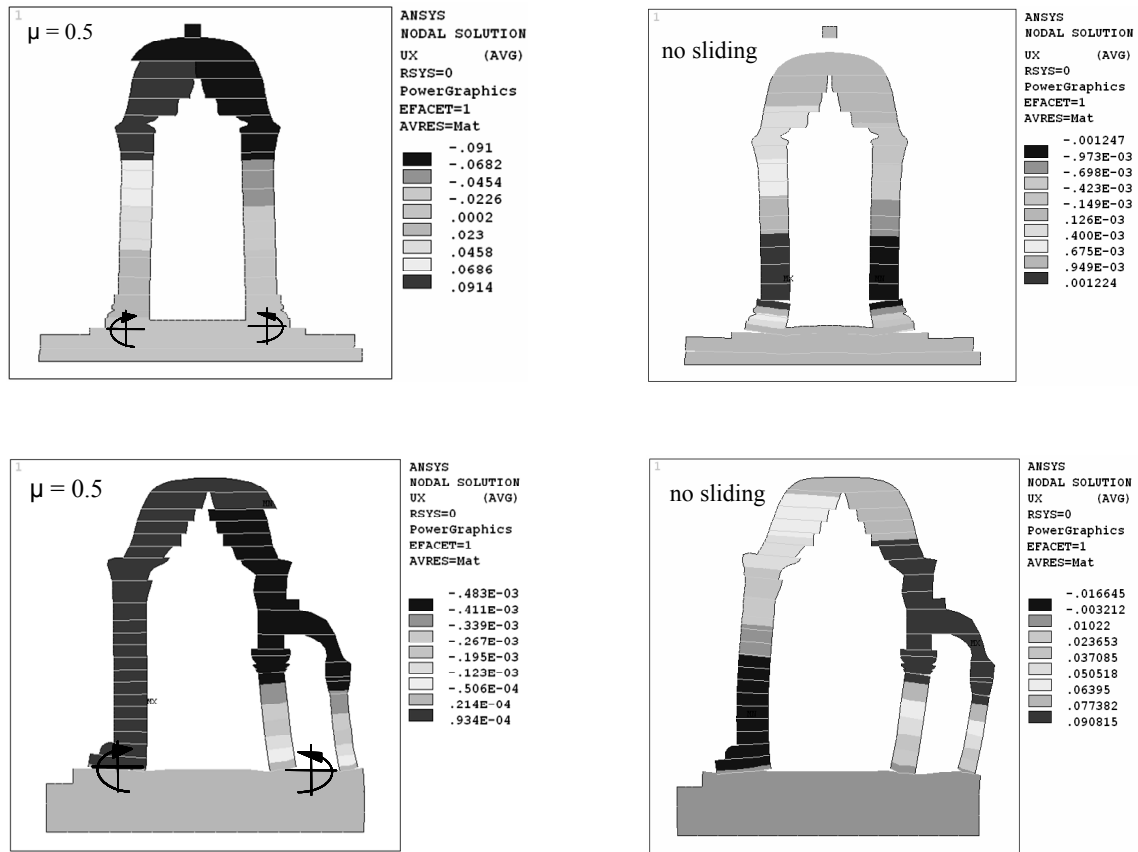


Figure 9 : Different failure modes in the first and second/third enclosure walls under inward rotation with different coefficient of friction

7 SUMMARY

The numerical analysis of the enclosure walls indicates that the failure of the structure can be attributed reasonably to rotational displacements at the foundations. The footing movements are mainly attributed to the penetration of the overgrowing tree roots. This study demonstrates the capability of non-linear finite elements methods to capture the sliding and rotational modes of failure in discontinuous materials as encountered in the unbonded stone masonry monuments at Angkor Wat in Cambodia.

REFERENCES

- Menon, D., Gandhi S R., Prasad, A M., Satyanarayana, K N., Mathews, M S., Chandran, S., Kanade, M M., Singh, S., et al. Technical Report on Preliminary studies on Structural, Geo-technical and Botanical aspects of Ta Prohm Temple at Siem Reap, Cambodia submitted to Archaeological Survey of India, January 2004.
- ANSYS, ANSYS Manual Set, ANSYS Inc., 275 Technology Drive, Canonburg, PA 15317, USA.
- Rooney, D.F. *ANGKOR An Introduction to Temples*, 4th Edition, Odyssey Publications Ltd, Hong Kong, 2004.
- Giordano, A., Mele, E. and Luca, D.A. 2002. *Modelling of historical masonry structures: Comparison of different approaches through a case study*. *Engineering Structures*, 24, p. 1057–1069.